Lower–Middle Ordovician carbon and oxygen isotope chemostratigraphy at Hällekis, Sweden

implications for regional to global correlation and palaeoenvironmental development

Lindskog, Anders; Eriksson, Mats E.; Bergström, Stig M.; Young, Seth A.

Published in:
Lethaia

DOI:
10.1111/let.12307

2019

"This is the peer reviewed version of the following article: Lindskog et al. 2019: Lower–Middle Ordovician carbon and oxygen isotope chemostratigraphy at Hällekis, Sweden: Implications for regional to global correlations and palaeoenvironmental development. Lethaia 52, 204–219., which has been published in final form at https://doi.org/10.1111/let.12307"

Lower–Middle Ordovician carbon and oxygen isotope chemostratigraphy at Hällekis, Sweden: Implications for regional to global correlations and palaeoenvironmental development

ANDERS LINDSKOG, MATS E. ERIKSSON, STIG M. BERGSTRÖM AND SETH A. YOUNG

Lindskog, A., Eriksson, M.E., Bergström, S.M. & Young, S.A. 2018: Lower–Middle Ordovician carbon and oxygen isotope chemostratigraphy at Hällekis, Sweden: Implications for regional to global correlations and palaeoenvironmental development. *Lethaia*, Vol. 52, pp. 204–219.

A high-resolution chemostratigraphic (coupled $\delta^{13}C_{carb}$ and $\delta^{18}O_{carb}$) study of the topmost Floian through the middle Darriwilian (Ordovician) succession at the Hällekis quarry, Kinnekulle, southern Sweden, shows relatively steady isotopic values with overall minor changes, although some notable short- and long-term shifts are discernible. A pronounced positive shift in $\delta^{13}C$ in the uppermost part of the study succession is identified as the Middle Darriwilian Isotopic Carbon Excursion (MDICE), representing the only named global isotopic excursion in the data set. Regional and global comparisons suggest that few details in the different carbon and oxygen isotope curves can be confidently correlated, but longer-term patterns appear quite consistent. Trends in the isotope data are also in agreement with palaeogeographic reconstructions. Differences in stratigraphic patterns of both carbon and oxygen isotopes between localities suggest strong secular development at several spatiotemporal scales; any global signal involving relatively minor isotopic shifts is often masked/subdued by local and regional overprinting and care should be taken not to overinterpret data sets. Collectively, the data suggest rising sea levels and cooling climates through the studied time interval, but detailed interpretations remain problematic. *Keywords: $\delta^{13}C$, $\delta^{18}O$, Dapingian, Darriwilian, 'Orthoceratite limestone', Correlation.*

Anders Lindskog [anders.lindskog@geol.lu.se] and Mats E. Eriksson [mats.eriksson@geol.lu.se], Department of Geology, Lund University, Sölvegatan 12, SE-22362 Lund, Sweden; Stig M. Bergström [bergstrom.1@osu.edu], School of Earth Sciences, The Ohio State University, 125 S. Oval Mall, Columbus, OH 43210, USA; Seth A. Young [sayoung2@fsu.edu], Department of Earth, Ocean, & Atmospheric Science and National High Magnetic Field Laboratory, Florida State University, Tallahassee, FL 32306-4520, USA.*

The Ordovician System has been the subject of intense palaeoenvironmental, palaeontologic and stratigraphic studies during the last few decades. These investigations have led to a more detailed understanding of the complexities of the faunal and environmental perturbations that occurred during this interval of the early Palaeozoic (e.g., Bergström et al. 2009). The Ordovician was a time of high global sea level, with expansive epeiric seas covering large parts of the palaeocontinents. In these shallow-water regions, there were remarkable changes in the global marine biota during the so-called Great Ordovician Biodiversification Event (GOBE), which resulted in numerous new taxa and the establishment of new ecologic niches (e.g., Webby et al. 2004; Servais et al. 2009; Algeo et al. 2016; Edwards & Saltzman 2016; Servais & Harper in press). By contrast, the last portion of the Ordovician Period is marked by the first of the big five mass extinction events, during which approximately 85% of all marine species are estimated to have disappeared (Jablonski 1991; Sheehan 2001; Harper et al. 2014).

In recent years, the overall view of the Ordovician climatic state has changed rather dramatically, from a 'Greenhouse world' to one with a climate that transitioned into conditions more similar to those of today (e.g., Frakes et al. 1992; Trotter et al. 2008). Detailed geochemical studies using refined

palaeotemperature proxies and modelling have led to a much more complex picture of Ordovician climate, including the recognition of several time intervals potentially representing ice ages (although glaciogenic deposits older than the latest Ordovician remain to be found; e.g., Trotter et al. 2008; Finnegan et al. 2011; Pohl et al. 2016; Rasmussen et al. 2016). Collectively, a surge of new biotic, sedimentologic, and geochemical data in recent decades has greatly improved our knowledge about this system, resulting in, among other things, the establishment of a robust and detailed chronostratigraphic framework with three global series and seven stages (e.g., Bergström et al. 2009; Cooper & Sadler 2012; Lindskog et al. 2017).

Various geochemical proxies, notably carbon isotopes ($\delta^{13}C$), have proven to be important for the development of global and regional stratigraphic correlations (e.g., Bergström et al. 2009). It is of crucial importance that the $\delta^{13}C$ chemostratigraphic framework is biostratigraphically well constrained, but distinctive isotopic shifts and excursions have proven to be important also for the correlation of strata in which biostratigraphically important fossils are rare or missing. However, great caution is needed in carrying out such correlations even at the regional scale (see Fanton & Holmden 2007; Schiffbauer et al. 2017). Despite the wealth of newly available stable isotopic data, more studies are needed in order to improve our understanding of their relations to palaeoenvironmental conditions and developments during the Ordovician, as well as their significance to the establishment of correlations at local, regional and global scales. For instance, problems persist in disentangling isostatic and eustatic signals in the global sea-level history (and by extension any associated climatic history). Accurate and detailed correlations are keys to the understanding abiotic and biotic events and processes at any larger spatiotemporal perspective.

The aim of the present study is to analyse the latest Floian through the middle Darriwilian carbon and oxygen stable-isotopic records at the Hällekis quarry in the Province of Västergötland in south-central Sweden. The Hällekis section is well studied in terms of biostratigraphy, sedimentology and event-stratigraphy, and is relatively expanded compared to most other coeval sections in Baltoscandia. This provides excellent possibilities to place the isotope data within local and regional palaeoenvironmental contexts of the Baltic palaeobasin, and its evolution throughout this time interval of the Ordovician. Here, we discuss and compare our results with previously studied stable isotopic profiles from coeval strata at both the regional and global scale.

Geological setting

During most of the early Palaeozoic, considerable parts of present-day northern Europe were covered by widespread epeiric seas (e.g., Torsvik & Cocks 2017). In Sweden and elsewhere on the Baltoscandian craton, a thin cover of sedimentary rocks records a long-term transgression (1st or 2nd order sea level cycle) that locally began in late Precambrian time (Fig. 1). During the Ordovician, much of Baltoscandia was covered by marine water in which net depositional rates were low (generally a few centimetres per thousand years; e.g., Lindström 1971). Surrounding landmasses were largely peneplained, with low relief resulting in limited transport of weathered terrigenous material into the basin. Bergström et al. (2011) calculated a net depositional rate for the 'orthoceratite limestone' (see below) at Kinnekulle of ~3.3 mm ka^{-1}, and Lindskog et al. (2017) calculated ~4 mm ka^{-1}.

Throughout the Ordovician, Baltica drifted from high southern latitudes into subtropical-tropical latitudes (Torsvik & Cocks 2017). On the Baltoscandian platform, most of the Ordovician was characterized carbonate deposition (e.g., Lindström 1971; Jaanusson 1973). The 'orthoceratite limestone', a condensed cool-water carbonate facies, comprises the main rock type in the Lower–Middle Ordovician succession on the Swedish craton. Today it occurs only in places where it has been protected from post-Ordovician erosion. Typically, the 'orthoceratite limestone' is reddish, brownish or grey in colour and consists of calcareous mud mixed with sand-sized skeletal grains and very limited amounts of terrigenous matter (e.g., Lindskog & Eriksson 2017, and references therein). Although nautiloid cephalopods, including orthoceratids, are common locally and lend their name to the informal rock unit, many parts of the 'orthoceratite limestone' do not contain abundant macrofossils. However, microfossils (notably conodonts) occur throughout the succession. The many cratonic outcrops in Sweden appear largely homogenous at the macroscopic scale and in Västergötland most outcrops are typically devoid of conspicuous evidence of tectonic activity (cf. Lindskog & Eriksson 2017, and references therein).

In Västergötland there are numerous outcrops of lower Palaeozoic strata and, because of past extensive quarrying, exposures of the 'orthoceratite limestone' are abundant. This is the case on Kinnekulle, an approximately 300-m high table mountain on the south-eastern shore of Lake Vänern (e.g., Holm & Munthe 1901; Munthe 1905; Priem et al. 1968). Here, the lower Palaeozoic marine succession, which rests on peneplained Precambrian gneiss, ranges from strata of the Cambrian Series 2 to the lower Llandovery, which is overlain by Permian dolerite. Kinnekulle can be regarded as the type area of the 'orthoceratite limestone' in Sweden (Hisinger 1828; Jaanusson 1982).

The Hällekis study interval ranges from the uppermost Floian Stage to the middle Darriwilian Stage (for stage terminology, see Bergström et al. 2009) and includes strata from the uppermost Lower to the middle part of the Middle Ordovician. The study succession begins in the uppermost Tøyen Shale, which ranges across the boundary between the Billingen and Volkhov Baltoscandian stages and corresponds to the uppermost part of Stage slice Fl3 of Bergström et al. (2009). The Tøyen Shale is overlain by the 'Lanna' and 'Holen' limestones, which are obsolete topoformations (i.e., historical units defined by a combination of lithology and fossil content; see Jaanusson 1960). Hence, these limestones are not lithostratigraphically defined and in lack of a revised lithostratigraphic framework they are herein retained as informal and provisional units (cf. Kumpulainen 2017; Lindskog & Eriksson 2017). The boundary between the Tøyen Shale and the 'Lanna Limestone' closely coincides with that between the Floian and Dapingian global stages (e.g., Bergström & Löfgren 2009). A conspicuous ~1.5-m-thick interval of grey limestone, informally known as the 'Täljsten', occurs across Kinnekulle in the lower part of the 'Holen Limestone' (see Lindskog & Eriksson 2017, and references therein). Disconformably overlying the 'Holen limestone' is the decimetre-thick 'Skövde Limestone', which belongs to the Lasnamägi Baltoscandian Stage and the Dw3 Stage slice of Bergström et al. (2009). The gap below the 'Skövde Limestone' corresponds to 2–3 conodont zones and some four million years of time (Zhang 1998a, b; Lindskog et al. 2017). This unit is overlain by the Gullhögen and Ryd formations of Uhaku age, which corresponds to the upper part of Stage slice Dw3. The basal beds of the Gullhögen Formation form the top of our study succession.

For this study we collected a composite section at the Hällekis quarry on the north-western slope of Kinnekulle (WGS 84 coordinates N58°36'33'', E13°23'42''; Figs. 1, 2). The same section and sample series were recently described in close detail for carbonate microfacies analyses and relative sea-level reconstructions by Lindskog & Eriksson (2017), allowing for direct comparison between data sets.

Materials and methods

A total of 220 limestone samples were collected through the measured Hällekis succession, spanning the uppermost Tøyen Shale through the basal Gullhögen Formation (Fig. 3; Lindskog & Eriksson 2017). The average space between the sample levels was ~15 cm. To obtain $\delta^{13}C_{carb}$ and $\delta^{18}O_{carb}$ values, the carbonate matrix of samples was preferentially targeted using a micro-drill to generate ~1 gram of powder, which was stored in clean micro-centrifuge tubes. Approximately 100–300 μg of carbonate powder were weighed into glass exetainer vials and then placed into a drying oven at 80°C for 8 h, in order to remove H_2O-vapor and any trace volatile organic compounds. These samples were then acidified with 3–5 drops of anhydrous phosphoric acid (H_3PO_4) in He purged, air tight exetainer vials. Samples were reacted with H_3PO_4 at 25°C for 24 h, and stable carbon and oxygen isotopic ratios of the evolved CO_2 were then measured using a Gas Bench II Autocarbonate device connected to a Thermo Delta Plus XP stable isotope ratio mass spectrometer (IRMS) at the National High Magnetic Field Laboratory at Florida State University. Carbon isotope ratios are corrected for ^{17}O contribution and reported in standard delta notation relative V-PDB (Vienna Pee Dee Belemnite) standard:

$$\delta^{13}C = [(^{13}C/^{12}C)_{sample}/(^{13}C/^{12}C)_{V\text{-}PDB}\text{-}1] \times 1000$$

$$\delta^{18}O = [(^{18}O/^{16}O)_{sample}/(^{18}O/^{16}O)_{V\text{-}PDB}\text{-}1] \times 1000$$

Our sample values are calibrated to international and FSU laboratory standards ROY-CC (+0.67‰, -12.02‰), MB-CC (-10.5‰, -3.5‰) NBS-19 (1.95‰, -2.2‰) and PDA (-1.3‰, -5.34‰) with standard deviations for $\delta^{13}C$ and $\delta^{18}O$ of ±0.05‰ and ±0.1‰, respectively (1 σ).

Results

The full dataset produced from the sample analyses is available in Table 1. The $\delta^{13}C_{carb}$ and $\delta^{18}O_{carb}$ values are plotted in Fig. 3, against the local stratigraphy and the inferred sea-level changes recognized by Lindskog & Eriksson (2017; see detailed discussion therein). In order to facilitate descriptions of the changes in isotopic values below, some intervals with distinct trends in the data are labelled C and O followed by a number. With the exception of the well documented Middle Darriwilian Isotopic Carbon Excursion (MDICE; see Ainsaar et al. 2010), we refrain from identifying these labelled shifts as named 'excursions' in order not to add to the already inflated number of minor isotopic kinks, or slight shifts from baseline values, identified as such in the Palaeozoic despite being of questionable correlative value and event-stratigraphic applicability. Hence, the letter-number scheme employed here for our observed trends in $\delta^{13}C_{carb}$ and $\delta^{18}O_{carb}$ may only have local to regional significance at this time due to many factors that effect these stable isotope records in shallow water carbonate platform settings (e.g., Holmden et al. 1998; Immenhauser et al. 2003; Panchuk et al. 2005; Swart 2008): water mass connectivity/restriction, pH, temperature, salinity, organic matter decomposition, $[CO_{2(aq)}]$, diagenesis, and carbonate mineralogy.

A carbon isotope profile at Hällekis quarry was previously documented by Schmitz et al. (2010), but their study only covered part of the 'orthoceratite limestone' succession and at relatively low stratigraphic resolution. Nonetheless, a comparison between the results of Schmitz et al. (2010) and the present study shows that the datasets match up well and that the $\delta^{13}C_{carb}$ curves coincide in terms of both stratigraphic pattern and value ranges. This attests to the reliability of the overall approach and data used while simultaneously comparing two different carbon isotope laboratories.

Carbon isotopes ($\delta^{13}C_{carb}$)

The $\delta^{13}C_{carb}$ values recorded are relatively uniform, mainly varying within the range of 0‰ to +1‰ throughout the study succession, although a long-term trend towards successively more positive values occurs up-section (Fig. 3). Beginning at the base of the studied succession, there is a marked albeit minor (~0.5‰) negative shift in values across the Billingen–Volkhov (~Floian–Dapingian) boundary interval, marked C1 in Fig. 3. This part of the local succession is characterized by abundant limonitic discontinuity surfaces (Lindskog & Eriksson 2017). A gradual trend towards more positive values (~1‰ magnitude shift) is seen throughout the lower Volkhovian. Within this general positive trend in $\delta^{13}C_{carb}$ values there is a relatively large scattering of data points that coincides with a distinct limestone-marl alternation interval in the 'Lanna Limestone' at Kinnekulle (between C1 and C2 in Fig. 3). A ~0.5 ‰ drop to lower $\delta^{13}C_{carb}$ values occurs in the middlemost Volkhovian (C2). This negative shift is not related to any obvious lithologic change, although detailed biotic and sedimentary facies analyses indicate a rise in the relative sea level (see Lindskog & Eriksson 2017). Succeeding $\delta^{13}C_{carb}$ values increase gradually up-section until a minor but marked negative shift occurs again close to the Volkhov–Kunda boundary (C3). These beds contain numerous limonitic discontinuity surfaces and limonite-stained grains, and locally derived intraclasts. The basal Kunda is associated with a rapid rise in $\delta^{13}C$ ‰ values. A slight but distinguishable decline to slightly lighter (~0.25‰ magnitude) values occurs in the middle Kunda interval (C4). This interval of lowered $\delta^{13}C_{carb}$ values coincides closely with the *M. hagetiana* subzone of the *L. pseudoplanus* conodont Zone (Zhang 1998a). It is followed up-section by increasingly higher values (up to +1.40‰) – with minor but pronounced rhythmic/cyclic fluctuations – leading into the MDICE interval. The onset of the MDICE is close to the base of the *M. ozarkodella* subzone of the *L. pseudoplanus* conodont Zone (ibid.) and is associated with a change into rocks with a clearly different lithology compared to those in the underlying strata, and the establishment of a pronounced alternation between limestone and marly/shaly interbeds (Lindskog & Eriksson 2017). The limestone of these strata is of exceptionally fine carbonate texture compared to that of the lower and middle parts of the 'Holen Limestone' and the fossil fauna is poor. The disconformable contact between the 'Holen Limestone' and the 'Skövde Limestone' is associated with a negative shift (~0.75‰ magnitude) in $\delta^{13}C_{carb}$ values, although the values increase again somewhat in the basal Gullhögen Formation (see also Schmitz et al. 2010). This part of the study succession is characterized by irregular beds and lenses of greyish limestone (~mudstone) and calcareous shale containing ferruginous and phosphatic ooids and skeletal debris (see Jaanusson 1964; Lindskog & Eriksson 2017).

Oxygen isotopes ($\delta^{18}O_{carb}$)

Most $\delta^{18}O_{carb}$ values vary between -7‰ and -6‰ throughout the succession, although there are some notable fluctuations (Fig. 3). Scatter within the $\delta^{18}O_{carb}$ data is typically quite pronounced, but more so in the lower Volkhovian than in the upper part of the succession. The transition between the Billingen and Volkhov Baltoscandian stages (Tøyen Shale–'Lanna Limestone') is associated with a distinct, ~0.5‰ magnitude shift into lower $\delta^{18}O_{carb}$ values, marked O1 in Fig. 3. The Volkhov Stage is thereafter characterized by relatively stable $\delta^{18}O_{carb}$ values scattering across a similar long-term mean. A distinct ~1‰ negative shift (from -6.5 to -7.5‰) in $\delta^{18}O_{carb}$ values is then seen across the Volkhov–Kunda boundary interval (O2). This is followed by a rapid rise in values in the lower Kunda interval, although relatively low values (-7.0‰) occur in the upper 'Täljsten' beds (O3), in the *A. expansus–A. raniceps* trilobite Zone and *L. variabilis–Y. crassus* conodont Zone boundary interval. After a sharp rise in the overlying strata to $\delta^{18}O_{carb}$ values near -6.0‰, a marked drop in values to -7.0‰ is then observed in the middle Kunda interval (O4), close to the base of the *M. ozarkodella* subzone of the *L. pseudoplanus* conodont Zone. This is associated with a gradual change in lithology, with the rocks becoming increasingly marly until the abovementioned limestone-marl/limestone-shale alternation is fully developed (see Lindskog & Eriksson 2017). The $\delta^{18}O_{carb}$ values are relatively stable, near -7.0‰, up section, but a consistent increase is observed in the uppermost Kunda beds (O5). The transition between the 'Holen Limestone' and the 'Skövde Limestone'–Gullhögen Formation is marked by a ~1.0‰ magnitude negative shift in $\delta^{18}O_{carb}$ values.

Discussion

The thermally and tectonically undisturbed strata of the 'orthoceratite limestone' at the Hällekis quarry appear to preserve a relatively good record of regional to global changes in marine $\delta^{13}C_{carb}$ and in part $\delta^{18}O_{carb}$. Several recently published papers deal with stratigraphic variations in $\delta^{13}C$ in successions coeval with the Hällekis study interval, but few have discussed the corresponding $\delta^{18}O$ records (although many studies include $\delta^{18}O$ datasets). In large part, this is likely due to the observation that $\delta^{18}O$ is relatively sensitive to lithologic variations and diagenetic alterations compared to $\delta^{13}C$ (e.g., Kah 2000; Melim et al. 2001; and references therein). The broad scattering of the Hällekis data points indicates that $\delta^{18}O_{carb}$ values are indeed strongly influenced by both lithologic characteristics and diagenetic processes, and thus less reliable for palaeoenvironmental interpretations and stratigraphic correlation than the corresponding $\delta^{13}C_{carb}$ data. Still, the stratigraphic patterns in the $\delta^{18}O_{carb}$ data show some clear similarities to those of other regional localities and different proxies that deserve closer inspection and discussion (see below).

As discussed recently in some detail by Saltzman & Edwards (2017), much information about the chemical and physical characteristics of the atmosphere and the oceans during the Ordovician remains to be unravelled. Carbon and oxygen isotopes, together with some other geochemical proxies, show promise to help in elucidating such information. However, in order to better understand the dynamics of long-term carbon and oxygen cycles of the Palaeozoic, great care must be exercised in assessing similarities and differences in stable-isotope datasets. With increasing distance from open oceanic settings, within the epeiric basins, comparisons at the global scale are likely to become more difficult due to increasingly restricted oceanographic circulation.

Here we first evaluate our new data within the context of factors that may affect the preservation of primary stable isotopic trends (i.e., diagenesis, carbonate mineralogy). Once established that our records reflect mostly primary Ordovician marine chemistry we go on to interpret these records in the context of factors that influence these stable isotopic data within shallow water carbonate platform settings: water mass restriction/connectivity, organic matter decomposition, temperature, salinity, and $[CO_{2(aq)}]$ (e.g., Holmden et al. 1998; Immenhauser et al. 2003; Panchuck et al. 2005; Swart 2008). With the aforementioned in mind, we explore possible changes to the regional to global environment (i.e., temperature, salinity, $[CO_{2(aq)}]$, burial flux of organic carbon) to produce these small but distinct changes in the $\delta^{13}C_{carb}$ and $\delta^{18}O_{carb}$ records from the Baltoscandian palaeobasin.

Diagenetic influence on the studied rocks

The 'orthoceratite limestone' at Kinnekulle typically shows evidence of early lithification and only very limited (late) diagenetic alteration (see Lindskog & Eriksson 2017, and references therein). The early lithification, together with a generally fine-grained composition and negligible primary and

secondary porosity, has ensured that the rocks have retained many of their original chemical and physical characteristics throughout time; few beds show any significant recrystallization effects and little interchange of materials between beds can be detected (e.g., Lindskog et al. 2017). The Kinnekulle area has largely been spared from tectonic disturbances throughout the Phanerozoic and the colour alteration index (~1) of conodonts from the 'orthoceratite limestone' reveal negligible heating of the rocks (e.g., Mellgren & Eriksson 2010). Cross plotting of the $\delta^{13}C$ and $\delta^{18}O$ data (Fig. 4) shows only limited correlation between numbers ($R^2 = 0.32$), indicating a general lack of influence from meteoric diagenesis (e.g., Allan and Matthews 1982; Jones et al. 2015). Possible meteoric influence is especially apparent close to some biostratigraphic boundaries, which likely coincide with slowed and/or temporarily halted deposition, although there are no (obvious) signs of subaerial exposure at Kinnekulle (Fig. 3). Even without meteoric influence, however, some correlation (positive or negative) can be expected if the two isotope systems were influenced by the same ambient environmental conditions and processes (see below). Original lithologic properties may also contribute. Collectively, the conditions suggest that the studied rocks retain relatively pristine records of carbon and oxygen isotopes.

Geographic comparisons and correlations

Coeval carbon isotope curves from Baltoscandian localities (outcrops and drill cores) often show consistent general patterns and trends, both in shorter and longer time perspectives (Fig. 5). The prominent negative shift (C1) in the lowermost Volkhov interval appears to be well reflected in successions that, like Kinnekulle, show a change in facies from argillaceous rocks to relatively pure limestone in this interval, but this shift is absent or poorly developed in successions completely dominated by limestone. As at Kinnekulle, many localities show a two-step (cyclic?) $\delta^{13}C$ development in the Volkhov Baltoscandian Stage. This can be observed as gradually increasing $\delta^{13}C$ values upward from the base to about the middle Volkhov, where there is a slight but marked temporary dip in values (C2) in the *Baltoniodus norrlandicus* conodont Zone (*sensu* Wu et al. 2017). Except in the most condensed successions, where this interval is characterized by a marked hiatus, a small magnitude (~0.5‰) negative shift in $\delta^{13}C_{carb}$ values (C3) is evident also near the Volkhov–Kunda boundary (the *Asaphus lepidurus*/*Megistaspis limbata–Asaphus expansus* trilobite Zone boundary). The succeeding Kunda Stage is consistently characterized by a gradual but fluctuating rise in $\delta^{13}C$ values, with another small magnitude negative shift of ~0.25–0.5‰ (C4) in the lower *Lenodus pseudoplanus* conodont Zone. This is followed by the geographically widespread and globally documented MDICE. A slight negative shift in $\delta^{13}C$ values is typically seen also in the topmost Kunda Stage, within the MDICE interval (the uppermost *L. pseudoplanus* Zone/lowermost *E. suecicus* conodont Zone; see also Lehnert et al. 2014). It appears that different 'phases' of the overall stratigraphic $\delta^{13}C$ development are of varying relative thickness throughout Baltoscandia, revealing important information on the spatiotemporal depositional dynamics in the regional palaeobasin – i.e., that different areas where characterized by deposition and/or erosion at different times. At Kinnekulle, the conspicuous hiatus below the 'Skövde Limestone' cuts out most of the MDICE (see also Schmitz et al. 2010). A corresponding stratigraphic gap can be traced along a belt southwards and into central Eastern Europe (and a similar gap also occurs elsewhere; e.g., Schmitz et al. 2010), but much of Baltoscandia experienced significant and essentially continuous deposition during this time (Fig. 5; Lindskog & Eriksson 2017).

Whilst most successions in Baltoscandia show similar overall $\delta^{13}C$ patterns through the Volkhov–Kunda interval, significant variations are observable between different areas and localities. For example, the Siljan area in Dalarna, central Sweden, deviates from other areas as it shows a long-term trend of strongly declining $\delta^{13}C$ values throughout the Volkhov Stage, that culminates in a pronounced low, or 'negative excursion', in values across the Volkhov–Kunda boundary (LDNICE of Lehnert et al. 2014; possibly a condensation-induced amalgamation of C3 and C4). Thereafter, the Kunda interval is characterized by a steady increase from baseline values leading directly into the MDICE (Ainsaar et al. 2010; Lehnert et al. 2014). In the Tingskullen drill core from northern Öland in south-eastern Sweden, the negative shift in $\delta^{13}C$ values that is characteristic of the middle Kunda (C4) is essentially not developed, whereas this shift is especially well pronounced in the Jämtland region, central Sweden, and in the easternmost Baltic successions (Ainsaar et al. 2010; Zaitsev & Pokrovsky 2014; Wu et al. 2015, 2017; Rasmussen et al. 2016). The $\delta^{13}C$ values are relatively low in western

Russia compared to those of other areas in the Baltoscandian palaeobasin (cf. Immenhauser et al. 2003). Variations in stratigraphic $\delta^{13}C$ patterns and values between different areas possibly reflect varying weathering sources and intensity of sediment input, and that all parts of the Baltoscandian palaeobasin were not always well connected in terms of oceanographic circulation and exchange with the open ocean (especially during lowstands; see Saltzman & Edwards 2017 and references therein). The timing and tempo of traceable changes also appears to differ somewhat (cf. Fanton & Holmden 2007; Schiffbauer et al. 2017; Rasmussen & Stouge 2018). These differences stress the need for caution when interpreting $\delta^{13}C$ curves in extreme high-resolution details, and highlight the importance of biostratigraphic control when correlating sections. Biostratigraphy in itself is obviously not without problems, however, as the timing of biostratigraphic boundaries appears to vary somewhat between well-studied sections (i.e., they are arguably asynchronous; e.g., Lindskog & Eriksson 2017).

Detailed comparisons between $\delta^{13}C$ curves become more problematic when expanding the scope to the global scale, although some general patterns appear to be recognizable (Fig. 5). The study interval is characterized by a long-term increase in $\delta^{13}C$ values in most successions, although there are exceptions and the amplitude of changes differs drastically between regions. Most significantly, datasets from the Great Basin in western USA and the Precordillera of Argentina show long-term standstill or even decrease in $\delta^{13}C$ values and the MDICE is not clearly discernible (cf. Albanesi et al. 2013; Saltzman & Edwards 2014, 2017; Henderson et al. 2018). Moreover, the stratigraphic patterns of $\delta^{13}C$ curves differ significantly between western USA, as represented by the Shingle Pass section in Nevada, and eastern USA, as represented by the Clear Spring section in Maryland; the long-term trends throughout the Dapingian–Darriwilian interval are essentially mirrored. Regardless of differences in stratigraphic patterns, both Argentinian and North American successions typically show distinctly lower $\delta^{13}C$ values compared to those from Baltoscandia. Whereas a minor part of this may be explained by temperature-dependent fractionation (e.g., Goericke & Fry 1994; Hayes et al. 1999) and other physical processes, most of the differences are likely due to global/regional differences in carbon stocks (e.g., Saltzman & Edwards 2017, and references therein). Furthermore, different sections appear to have been strongly influenced by local physical and chemical syn- and post-depositional conditions.

Although the data scatter conspicuously, most sections in Baltoscandia appear to record the same overall trend in $\delta^{18}O$ values (Fig. 6). The study interval is characterized by a long-term rise in $\delta^{18}O$ values with recurring (cyclic?) negative shifts that appear traceable between sections. The amplitude of variations is much less distinct in Jämtland than in other parts of Baltoscandia. This likely reflects that the Jämtland area was a relatively deep-water setting, but the relatively moderate scattering in the Brunflo 2 drill core data may also indicate homogenization during diagenesis (‘resetting’; cf. Wu et al. 2015). The data from the Mehikoorma 421 drill core in Estonia differ drastically from the other Baltoscandian datasets in that the post-Kunda interval is characterized by relatively low $\delta^{18}O$ values. The data from the USA also show a long-term trend of increasing $\delta^{18}O$ values, although with distinct differences in stratigraphic range/position and amplitude of changes between sections. Curiously, Clear Spring shows a similar small magnitude drop in $\delta^{18}O$ values approximately through the same stratigraphic interval as in Mehikoorma 421. Despite the susceptibility of oxygen isotopes to alteration, data from bulk carbonates show remarkably similar patterns to that produced from conodont elements and brachiopod shells (Trotter et al. 2008; Zaitsev & Pokrovsky 2014; Rasmussen et al. 2016). There is a tendency for bimodality in the $\delta^{18}O$ values in some parts of the Hällekis succession, with a marked and potentially systematic difference between minimum and maximum values in the data scatter, as can also be observed in the Tingskullen drill core (Fig. 6). This may reflect high-frequency palaeoenvironmental and/or diagenetic variations.

A distinct trend is observed in the $\delta^{18}O$ data across Baltoscandia, wherein values become lower roughly from east to west; values typically vary between ~-4 and -5‰ in the easternmost part of the region (western Russia), and between ~-8 and -10‰ in its western parts (Fig. 6; cf. Immenhauser et al. 2003). Assuming that $\delta^{18}O$ reflects water temperature in the depositional environment, the data suggest a gradient of ~15–20° C (Epstein et al. 1953) with warmer water to the west. This may seem to be in contrast with what can be intuitively expected as water generally became deeper and more oceanic in western direction, and thus likely colder, especially when considering potential upwelling areas (e.g., Lindström & Vortisch 1983; Rasmussen et al. 2016; cf. Lindström 1984). However, palaeogeographic reconstructions show that the present-day western edge of Baltica was oriented

northwards in the Middle Ordovician (e.g., Torsvik & Cocks 2017). Thus, this part of the palaeocontinent was facing the Iapetus Ocean and the regional trend in $\delta^{18}O$ could reflect increasing exposure to warmer waters coming in from lower latitudes. Conodont biofacies analyses support this interpretation (Rasmussen & Stouge 2018), although further studies are needed in order to elucidate what (and how) other factors and processes may have influenced the observed $\delta^{18}O$ trends. In the USA, $\delta^{18}O$ values span the entire range of those seen in Baltoscandia and stratigraphic variations are somewhat contradictory (Fig. 6). This suggests that specific values do not translate directly into temperature, as Laurentia was consistently situated in distinctly warmer latitudes as compared to most of Baltica (e.g., Torsvik & Cocks 2017), and the amplitude of variations in $\delta^{18}O$ indicates relatively complex depositional and/or diagenetic histories compared to sections elsewhere. The similarity between different $\delta^{18}O$ data sets and trends indicates that bulk rock oxygen isotopes commonly retain primary signals and, thus, may provide valuable palaeoenvironmental information that is rarely acknowledged or even discussed in recent literature (cf. Lindström 1984).

Carbon and oxygen isotopes vs. palaeoenvironmental development

Comparison between isotopic, palaeontologic and sedimentologic data (see Lindskog & Eriksson 2017, and references therein) from the Hällekis quarry indicate a near inverse relationship between carbon isotope values and estimated relative sea level through most of the study interval, although the labelled shifts (C1–C4) deviate from this general pattern (Fig. 3). This probably reflects that times of higher sea level were associated with influx of more open marine waters into the Baltoscandian palaeobasin and that lowstands (and shallower-water areas in general) were associated with a more 'regional' and variable $\delta^{13}C$ signal (e.g., Immenhauser et al. 2002, 2003; Bergström et al. 2011; Edwards & Saltzman 2014). Oxygen isotopes also appear to have co-varied with relative sea level, although scattering and variability in the data preclude confident interpretations. It is noteworthy, however, that the coincident patterns suggest that temperature (and its influence on water and ice volumes) was an important driver of sea level change and the global data supports interpretations of a cooling trend through the studied time interval (see below; e.g., Trotter et al. 2008; Rasmussen et al. 2016). Correlation between sea level and isotopic values is also implied at higher frequencies, but scatter in the isotope data precludes confident interpretation.

The apparent pattern of inverse co-variation between $\delta^{13}C$ values and sea level is decoupled in the uppermost part of the study succession, when entering into the MDICE interval. This occurs in association with a marked lithological change at Kinnekulle, as is also the case in many other areas of Sweden. The collective results and observations suggest migration of the regional depocenter(s) into the interior parts of the Baltoscandian craton, likely as a result of rising sea level (see detailed discussion in Lindskog & Eriksson 2017). This may have changed the conditions for the circulation and transport across the palaeobasin, here reflected in a shift in the relationship between $\delta^{13}C$ and sea level. The widespread development of the MDICE is consistent with a global rise in sea level, as continents were extensively flooded and epeiric seas brought into better contact with isotopically heavier oceanic water masses (e.g. Allan & Matthews 1982; Patterson & Walter 1994; Immenhauser et al. 2003; Fanton & Holmden 2007). A net trend of rising sea level through the MDICE interval has been inferred globally, although exceptions occur locally (e.g., Barnes 1984; Haq & Schutter 2008; Agematsu & Sashida 2009; Dronov et al. 2009; Saltzman & Edwards 2017; Henderson et al. 2018). However, it remains difficult to disentangle epeirogenic/isostatic signals from eustatic ones at higher resolutions. The expression of the MDICE may have been enhanced by changes in bioproductivity and carbon burial due to increasing shelf areas (e.g., Fanton & Holmden 2007). The predominantly small magnitude shifts in Middle Ordovician stable carbon isotopes suggest that changes in the global burial fluxes of carbon were likely small in magnitude as compared to, for example, the Late Ordovician–Silurian interval, which is characterized by multiple large-magnitude positive excursions (e.g., Saltzman 2005).

The most distinct deviations in both carbon and oxygen isotopic values (C1–C4, O1–O5; Figs. 5, 6) coincide with notable palaeontologic and/or sedimentologic changes in the Baltoscandian palaeobasin, reasonably related to changes in sea level (e.g., Bergström et al. 2013; Lindskog & Eriksson 2017; Rasmussen & Stouge 2018; and references therein). As such, the typically negative shifts appear to reflect times of increased riverine input into the palaeobasin during lowstand conditions. The amplitude of changes tends to increase into the shallower (and/or proximal) parts of the palaeobasin

(Fig. 1), likely as a combined result of more biotic and hydrodynamic activity and a general decrease in stratigraphic completeness due to increasing condensation and the presence of more stratigraphic gaps.

The long-term trends in ^{18}O at the global scale suggest a cooling climate through the studied time interval, theoretically of some 5–10° C in average temperature (Epstein et al. 1953), although these numbers unrealistically assume a lack of other influences (e.g., variations in evaporation, input of weathering products, differential diagenesis) on $\delta^{18}O$ in all concerned rock sections. Nevertheless, the notion of a cooling climate during the Middle Ordovician is consistent with interpretations by, for example, Trotter et al. (2008), Pohl et al. (2016), Rasmussen et al. (2016) and Rasmussen & Stouge (2018).

However interpreted, disentangling one palaeoenvironmental signature from another and/or from diagenetic ones remains a complex and problematic task that is often impossible with $\delta^{13}C_{carb}$ and $\delta^{18}O_{carb}$ data sets alone.

Conclusions

A high-resolution chemostratigraphic (coupled $\delta^{13}C_{carb}$ and $\delta^{18}O_{carb}$) study of the topmost Floian through the middle Darriwilian succession at the Hällekis quarry, Kinnekulle, southern Sweden shows relatively steady isotopic values, although some notable short-term and long-term shifts are discernible. The only confidently identified shift from 'baseline' values, currently regarded as a true (named) global isotopic excursion, is the positive MDICE.

Comparison between Middle Ordovician datasets from various localities worldwide suggests that smaller magnitude (~0.25–0.5‰) and shorter duration (10–>100 kyr) shifts in different carbon and oxygen isotope curves cannot be confidently correlated in most cases, although longer-term (≥Myr time scales) and broader patterns appear quite consistent, especially at the regional scale. The differences in stratigraphic patterns of both carbon and oxygen isotopes between localities suggest strong secular development at several spatiotemporal scales, and global perturbations of the carbon cycle that resulted in isotopic shifts <1% in magnitude are often masked/subdued by local and regional water mass and diagenetic effects. Efforts to construct composite 'reference standards' for chemostratigraphic purposes must take into account geographic variability. Still, the stable isotope datasets support the growing body of proxy evidence suggesting progressive cooling of the Middle Ordovician oceans (e.g., Trotter et al. 2008; Rasmussen et al. 2016) and that redox conditions oscillated from oxic to dysoxic/anoxic in parts of the ocean (e.g., Young et al. 2016). Moreover, our results suggest that isotope data, in addition to forming a powerful correlation tool, can help in elucidating palaeogeographic scenarios.

Robust interpretation of the climatic development and its specific parameters in terms of more absolute numbers remains hampered by different tectonic histories of the palaeocontinents, and the restriction and poor circulation across intracratonic basins causes problems in disentangling global carbon and oxygen conditions from the often conflicting local, regional and global patterns. Moreover, due to the marked faunal provincialism and associated lack of common key index fossils during the Ordovician, precise biostratigraphic correlations of geographically widely separated successions are often difficult. In the absence of good biostratigraphic control of study successions, detailed comparison of isotope curves from different localities is unlikely to produce very reliable results.

Acknowledgements. – This study was funded by the American Chemical Society Petroleum Research Fund (grant ACS-PRF# 57487-DNI2 to S.A.Y.), the Birgit and Hellmuth Hertz' Foundation and the Royal Physiographic Society in Lund (N.M.T. grant to A.L.) and the Swedish Research Council (grant no. 2015-05084 to M.E.E.). We thank Chelsie Bowman and Nevin Kozik at Florida State University for assistance with stable isotopic analyses. Geochemical work was performed at the National High Magnetic Field Laboratory, which is supported by the National Science Foundation Cooperative Agreement No. DMR-1157490 and the State of Florida. Jan A. Rasmussen and an anonymous reviewer are thanked for thorough and thoughtful reviews, which helped to greatly strengthen the final manuscript. This paper is a contribution to IGCP project 653 – 'The onset of the Great Ordovician Biodiversification Event'.

References

Agematsu, , S. & Sashida, K. 2009: Ordovician sea-level change and paleogeography of the Sibumasu Terrane based on the conodont biostratigraphy. *Paleontological Research 13*, 327–336.

Ainsaar, L., Meidla, T., Tinn, O. 2004. Middle and Upper Ordovician stable isotope stratigraphy across the facies belts in the East Baltic. *In* O. Hints & L. Ainsaar, L. (eds.): *WOGOGOB-2004 Conference Materials*. Tartu University Press, Tartu, 11–12.

Ainsaar, L., Kaljo, D., Martma, T., Meidla, T., Männik, P., Nõlvak, J. & Tinn, O. 2010: Middle and Upper Ordovician carbon isotope chemostratigraphy in Baltoscandia: a correlation standard and clues to environmental history. *Palaeogeography, Palaeoclimatology, Palaeoecology 294*, 189–201.

Albanesi, G.L., Bergström, S.M., Schmitz, B., Serra, F., Feltes, N.A., Voldman, G.G. & Ortega, G. 2013: Darriwilian (Middle Ordovician) $\delta^{13}C_{carb}$ chemostratigraphy in the Precordillera of Argentina: Documentation of the middle Darriwilian Isotope Carbon Excursion (MDICE) and its use for intercontinental correlation. *Palaeogeography, Palaeoclimatology, Palaeoecology 389*, 48–63.

Algeo, T. J., Marenco, P. J., Saltzman, M. R. 2016. Co-evolution of oceans, climate, and the biosphere during the 'Ordovician Revolution': A review. *Palaeogeography, Palaeoclimatology, Palaeoecology 458*, 1–11.

Allan, J.R. & Matthews, R.K. 1982: Isotope signatures associated with early meteoric diagenesis. *Sedimentology 29*, 797–817.

Barnes, C.R. 1984: Early Ordovician eustatic events in Canada. *In* D.L. Bruton (ed.): Aspects of the Ordovician System. *Palaeontological Contributions from the University of Oslo 295*, 51–63.

Bergström, J., Pärnaste, H. & Zhou, Z.-Y. 2013: Trilobites and biofacies in the Early–Middle Ordovician of Baltica and a brief comparison with the Yangtze Plate. *Estonian Journal of Earth Sciences 62*, 205–230.

Bergström, S.M. 2007: The Ordovician conodont biostratigraphy in the Siljan region, south-central Sweden: a brief review of an international reference standard. *In* J.O Ebbestad, L. Wickström & A. Högström (eds.): *WOGOGOB 2007, 9th meeting of the Working Group on Ordovician Geology of Baltoscandia, Field guide and abstracts, Sveriges Geologiska Undersökning Rapporter och Meddelanden 128* 26–41.

Bergström, S.M. & Löfgren, A. 2009: The base of the global Dapingian Stage (Ordovician) in Baltoscandia: conodonts, graptolites and unconformities. *Earth and Environmental Science Transactions of the Royal Society of Edinburgh 99 (for 2008)*, 189–212.

Bergström, S.M., Chen, X., Gutiérrez-Marco, J.C. & Dronov, A. 2009: The new chronostratigraphic classification of the Ordovician System and its relations to major regional series and stages and to $\delta^{13}C$ chemostratigraphy. *Lethaia 42*, 97–107.

Bergström, S.M., Calner, M., Lehnert, O. & Noor, A. 2011: A new upper Middle Ordovician–Lower Silurian drillcore standard succession from Borenshult in Östergötland, southern Sweden: 1. Stratigraphical review with regional comparisons. *GFF 133*, 149–171.

Cooper, R.A. & Sadler, P.M. 2012: The Ordovician Period. In F.M. Gradstein, J.G. Ogg, M. Schmitz & G. Ogg: *The Geologic Time Scale 2012*, 489–523. Elsevier, Amsterdam.

Dronov, A.V., Kanygin, A.V., Timokhin, A.V., Tolmacheva, T.Yu. & Gonta, T.V. 2009: Correlation of eustatic and biotic events in the Ordovician paleobasins of the Siberian and Russian platforms. *Paleontological Journal 43*, 1477–1497.

Edwards, C.T. & Saltzman, M.R. 2014: Carbon isotope ($\delta^{13}C_{carb}$) stratigraphy of the Lower–Middle Ordovician (Tremadocian–Darriwilian) in the Great Basin, western United States: Implications for global correlation. *Palaeogeography, Palaeoclimatology, Palaeoecology 399*, 1–20.

Edwards, C.T. & Saltzman, M.R. 2016: Paired carbon isotopic analysis of Ordovician bulk carbonate ($\delta^{13}C_{carb}$) and organic matter ($\delta^{13}C_{org}$) spanning the Great Ordovician Biodiversification Event. *Palaeogeography, Palaeoclimatology, Palaeoecology 458*, 102–117.

Epstein, S., Buchsbaum, R., Lowenstam, H.A. & Urey, H.C. 1953: Revised carbonate-water isotopic temperature scale. *Bulletin of the Geological Society of America 64*, 1315–1326.

Fanton, K.C. & Holmden, C. 2007: Sea-level forcing of carbon isotope excursions in epeiric seas: implications for chemostratigraphy. *Canadian Journal of Earth Sciences 44*, 807–818.

Finnegan, S., Bergmann, K., Eiler, J.M., Jones, D.S., Fike, D.A., Eisenman, I., Hughes, N.C., Tripati, A.K. & Fischer, W.W. 2011: The magnitude and duration of Late Ordovician–Early Silurian Glaciation. *Science 331*, 903–906.

Frakes, L.A., Francis, J.E. & Syktus, J.I., 1992: *Climatic modes of the Phanerozoic*. Cambridge University Press, Cambridge. 274 pp.

Goericke, R. & Fry, B. 1994: Variations of marine plankton $\delta^{13}C$ with latitude, temperature, and dissolved CO2 in the world ocean. *Global Geochemical Cycles 8*, 85–90.

Harper, D.A.T., Hammarlund, E.U. & Rasmussen, C.M.Ø. 2014: End Ordovician extinctions: A coincidence of causes. *Gondwana Research 25*, 1294–1307.

Hayes, J.M., Strauss, H. & Kaufman, A.J. 1999: The abundance of ^{13}C in marine organic matter and isotopic fractionation in the global biogeochemical cycle of carbon during the past 800 Ma. *Chemical Geology 161*, 103–125.

Haq, B.U. & Schutter, S.R. 2008: A chronology of Paleozoic sea-level changes. *Science 322*, 64–68.

Henderson, M.A., Serra, F., Feltes, N.A., Albanesi, G.A. & Kah, L.C. 2018: Paired isotope records of carbonate and organic matter from the Middle Ordovician of Argentina: Intrabasinal variation and effects of the marine chemocline. *Palaeogeography, Palaeoclimatology, Palaeoecology 490*, 107–130.

Hisinger, W. 1828: *Anteckningar i physik och geognosi under resor uti Sverige och Norrige, Fjerde häftet*. Elméns och Granbergs tryckeri, Stockholm. 260 pp.

Holm, G. & Munthe, H. (eds.) 1901: Kinnekulle: Dess geologi och den tekniska användningen af dess bergarter. *Sveriges Geologiska Undersökning C172*, 1–144.

Holmden, C., Creaser, R.A., Muehlenbachs, K., Leslie, S.A. & Bergström, S.M. 1998: Isotopic evidence for geochemical decoupling between ancient epeiric seas and bordering oceans: implications for secular curves. *Geology 26*, 567–570.

Immenhauser, A., Kenter, J.A.M., Ganssen, G., Bahamonde, J.R., van Vliet, A. & Saher, M.H. 2001: Origin and significance of isotope shifts in Pennsylvanian carbonates (Asturias, NW Spain). *Journal of Sedimentary Research 72*, 82–94.

Immenhauser, A., Della Porta, G., Kenter, J.A.M. & Bahamonde, J.R. 2003: An alternative model for positive shifts in shallow ‐ marine carbonate $\delta^{13}C$ and $\delta^{18}O$. *Sedimentology 50*, 953–959.

Jaanusson, V. 1960: The Viruan (Middle Ordovician) of Öland. *Bulletin of the Geological Institutions of the University of Uppsala 38*, 207–88.

Jaanusson, V. 1964: The Viruan (Middle Ordovician) of Kinnekulle and Northern Billingen, Västergötland. *Bulletin of the Geological Institutions of the University of Uppsala 43*, 1–73.

Jaanusson, V. 1973: Aspects of carbonate sedimentation in the Ordovician of Baltoscandia. *Lethaia 6*, 11–34.

Jaanusson, V. 1982: Ordovician in Västergötland. *In* D.L. Bruton and S.H. Williams (eds.): Field Excursion Guide. 4th International Symposium on the Ordovician System. *Paleontological Contributions from the University of Oslo 279*, 164–183.

Jaanusson, V. & Mutvei, H. 1951: Ein Profil durch den Vaginatum-Kalkstein im Siljan-Gebiet, Dalarna. *Geologiska Föreningens i Stockholm Förhandlingar 73*, 630–636.

Jablonski, D. 1991: Extinctions: a paleontological perspective. *Science 253*, 754–57

Jones, D.S., Creel, R.C., Rios, B. & Ramos, D.P.S. 2015: Chemostratigraphy of an Ordovician–Silurian carbonate platform: $\delta^{13}C$ records below glacioeustatic exposure surfaces. *Geology 43*, 59–62.

Kah, L.C. 2000: Depositional $\delta^{18}O$ signatures in Proterozoic dolostones: constraints on seawater chemistry and early diagenesis. *SEPM Special Publication 67*, 345–360.

Kaljo, D., Martma, T. & Saadre, T. 2007: Post-Hunnebergian Ordovician carbon isotope trend in Baltoscandia, its environmental implications and some similarities with that of Nevada. *Palaeogeography, Palaeoclimatology, Palaeoecology 245*, 138–155.

Karis, L. 1998: Jämtlands östliga fjällberggrund. *In* L. Karis and A.G.B. Strömberg (eds.): Beskrivning till berggrundskartan över Jämtlands län, Del 2: Fjälldelen. *Sveriges Geologiska Undersökning Ca53:2*, 1–184.

Kumpulainen, R.A. (ed.) 2017: Guide for geological nomenclature in Sweden. *GFF 139*, 3–20.

Lehnert, O., Meinhold, G., Wu, R., Calner, M. & Joachimski, M.M. 2014: $\delta^{13}C$ chemostratigraphy in the upper Tremadocian through lower Katian (Ordovician) carbonate succession of the Siljan district, central Sweden. *Estonian Journal of Earth Sciences 63*, 277–286.

Lindskog, A. & Eriksson, M.E. 2017: Megascopic processes reflected in the microscopic realm: sedimentary and biotic dynamics of the Middle Ordovician "orthoceratite limestone" at Kinnekulle, Sweden. *GFF 139*, 163–183.

Lindskog, A., Eriksson, M.E. & Pettersson, A.M.L. 2014: The Volkhov–Kunda transition and the base of the Holen Limestone at Kinnekulle, Västergötland, Sweden. *GFF 136*, 167–171.

Lindskog, A., Costa, M.M., Rasmussen, C.M.Ø., Connelly, J.N. & Eriksson, M.E. 2017: Refined Ordovician timescale reveals no link between asteroid breakup and biodiversification. *Nature Communications 8*, 14066 (doi: 10.1038/ncomms14066).

Lindström, M. 1971: Vom Anfang, Hochstand und Ende eines Epikontinentalmeeres. *Geologische Rundschau 60*, 419–438.

Lindström, M. 1984: The Ordovician climate based on the study of carbonate rocks. *In* Bruton, D.L. (ed.): *Aspects of the Ordovician System. Palaeontological Contributions from the University of Oslo 295*, 81–88.

Lindström, M. & Vortisch, W. 1983: Indications of upwelling in the Lower Ordovician of Scandinavia. *In* J. Thiede & E. Suess (eds.): *Coastal upwelling*, 535–551. Plenum, New York.

Löfgren, A. 1995: The middle Lanna/Volkhov Stage (middle Arenig) of Sweden and its conodont fauna. *Geological Magazine 132*, 693–711.

Löfgren, A. 2003: Conodont faunas with *Lenodus variabilis* in the upper Arenigian to lower Llanvirnian of Sweden. *Palaeontologica Polonica 48*, 417–436.

Meidla, T., Ainsaar, L., Backman, J., Dronov, A., Holmer, L. & Sturesson, U. 2004: Middle–Upper Ordovician carbon isotopic record from Västergötland (Sweden) and East Baltic. *In* O. Hints & L. Ainsaar, L. (eds.): *WOGOGOB-2004 Conference Materials*. Tartu University Press, Tartu, 67–68.

Melim, L.A., Swart, P.K. & Maliva, R.G. 2001: Meteoric and marine-burial diagenesis in the subsurface of Great Bahama Bank. *SEPM Special Publication 70*, 137–161.

Mellgren, J.I.S. & Eriksson, M.E. 2010: Untangling a Darriwilian (Middle Ordovician) palaeoecological event in Baltoscandia: conodont faunal changes across the 'Täljsten' interval. *Earth and Environmental Science Transactions of the Royal Society of Edinburgh 100*, 353–370.

Munthe, H. 1905: De geologiska hufvuddragen af Västgötabergen och deras omgifning. *Geologiska Föreningens i Stockholm Förhandlingar 27*, 347–401.

Nielsen, A.T. 1995: Trilobite systematics, biostratigraphy and palaeoecology of the Lower Ordovician Komstad Limestone and Huk formations, southern Scandinavia. *Fossils and Strata 38,* 1–374.

Panchuk, K.M., Holmden, C. & Kump, L.R. 2005: Sensitivity of the epeiric sea carbon-isotope record to local-scale carbon cycle processes: Tales from the Mohawkian Sea. *Palaeogeography, Palaeoclimatology, Palaeoecology 228*, 320–337.

Patterson, W.P. & Walter, L.M. 1994: Depletion of ^{13}C in seawater ΣCO_2 on modern carbonate platforms: Significance for the carbon isotopic record of carbonates. *Geology 22*, 885–888.

Pohl, A., Donnadieu, Y., Le Hir, G., Ladant, J.-B., Dumas, C., Alvarez-Solas, J. & Vandenbroucke, T.R.A. 2016: Glacial onset predated Late Ordovician climate cooling. *Paleoceanography 31*, 800–821.

Priem, H.N.A., Mulder, F.G., Boelrijk, N.A.I.M., Hebeda, E.H., Verschure, R.H. & Verdurmen, E.A.T. 1968: Geochronological and palaeomagnetic reconnaissance survey in parts of central and southern Sweden. *Physics of the Earth and Planetary Interiors 1*, 373–380.

Rasmussen, C.M.Ø., Ullmann, C.V., Jakobsen, K.G., Lindskog, A., Hansen, J., Hansen, T., Eriksson, M.E., Dronov, A., Frei, R., Korte, C., Nielsen, A.T. & Harper, D.A.T. 2016: Onset of main Phanerozoic marine radiation sparked by emerging Mid Ordovician icehouse. *Scientific Reports 6*, 18884 (doi: 10.1038/srep18884).

Rasmussen, J.A. & Stouge, S. 2018: Baltoscandian biofacies and their link to Middle Ordovician (Darriwilian) global cooling. *Palaeontology 61*, 391–416.

Saltzman, M.R. 2005: Phosphorus, nitrogen, and the redox evolution of the Paleozoic oceans. *Geology 33*, 573–576.

Saltzman, M.R. & Edwards, C.T. 2017; Gradients in the carbon isotopic composition of Ordovician shallow water carbonates: A potential pitfall in estimates of ancient CO_2. *Earth and Planetary Science Letters 464*, 46–54.

Schiffbauer, J.D., Huntley, J.W., Fike, D.A., Jeffrey, M.J., Gregg, J.M. & Shelton, K.L. 2017: Decoupling biogeochemical records, extinction, and environmental change during the Cambrian SPICE event. *Science Advances 3*, e1602158.

Schmitz, B., Bergström, S.M. & Xiaofeng, W. 2010: The middle Darriwilian (Ordovician) $\delta^{13}C$ excursion (MDICE) discovered in the Yangtze Platform succession in China: implications of its first recorded occurrences outside Baltoscandia. *Journal of the Geological Society 167*, 249–259.

Servais, T. & Harper, D.A.T. in press: The Great Ordovician Biodiversification Event (GOBE); definition, concept and duration. *Lethaia* (DOI: 10.1111/let.12259).

Servais, T., Harper, D.A.T., Li, J., Munnecke, A., Owen, A.W., Sheehan, P.M. 2009. Understanding the Great Ordovician Biodiversification Event (GOBE): Influences of paleogeography, paleoclimate, or paleoecology? *GSA Today 19*, 4–10.

Sheehan, P.M. 2001: The Late Ordovician mass extinction. *Annual Review of Earth and Planetary Sciences 29*, 331–364.

Swart, P.K. 2008: Global synchronous changes in the carbon isotopic composition of carbonate sediments unrelated to changes in the global carbon cycle. *PNAS 105*, 13741–13745.

Tjernvik, T. 1956: On the early Ordovician of Sweden. Stratigraphy and fauna. *Bulletin of the Geological Institutions of the University of Uppsala 36*, 107–284.

Torsvik, T.H. & Cocks, L.R.M. 2017: Earth History and Palaeogeography. Cambridge University Press, Oxford. 317 pp.

Trotter, J.A., Williams, I.S., Barnes, C.R., Lécuyer, C. & Nicoll, R.S. 2008: Did cooling oceans trigger Ordovician biodiversification? Evidence from conodont thermometry. *Science 321*, 550–554.

Webby, B.D., Paris, F., Droser, M.L. & Percival, I.G. (eds.) 2004: *The Great Ordovician Biodiversification Event*. Columbia University Press, New York. 484 pp.

Wu, R., Calner, M., Lehnert, O., Peterffy, O., Joachimski, M.M. 2015: Lower–Middle Ordovician $\delta^{13}C$ chemostratigraphy of western Baltica (Jämtland, Sweden). *Palaeoworld 24*, 110–122.

Wu, R., Calner, M. & Lehnert, O. 2017: Integrated conodont biostratigraphy and carbon isotope chemostratigraphy in the Lower–Middle Ordovician of southern Sweden reveals a complete record of the MDICE. *Geological Magazine 154*, 334–353.

Young, S.A., Gill, B.C., Edwards, C.T., Saltzman, M.R. & Leslie, S.A. 2016: Middle–Late Ordovician (Darriwilian–Sandbian) decoupling of global sulfur and carbon cycles: isotopic evidence from eastern and southern Laurentia. *Palaeogeography, Palaeoclimatology, Palaeoecology* 458, 118–132.

Zaitsev, A.V. & Pokrovsky, B.G. 2014: Carbon and oxygen isotope compositions of Lower–Middle Ordovician carbonate rocks in the northwestern Russian Platform. *Lithology and Mineral Resources 49*, 272–279.

Zhang, J. 1998a: Middle Ordovician conodonts from the Atlantic Faunal Region and the evolution of key conodont genera. *Meddelanden från Stockholms universitets institution för geologi och geokemi 298*, 27 pp.

Zhang J. 1998b: The Ordovician conodont genus *Pygodus*. *In* H. Szaniawski (ed.): Proceedings of the Sixth European Conodont Symposium (ECOS VI). *Palaeontologia Polonica 58*, 87–105.

FIGURES AND TABLE

Fig. 1. Map of the Baltoscandian region (modified from Lindskog & Eriksson 2017). Geographic areas (e.g., localities, provinces) referred to in the main text and succeeding figures are shown. The distribution of lower Palaeozoic rocks is shown by green shading; areas with significant outcrops of Ordovician strata are indicated by darker shading. Generalized, the shelf became deeper from east to west and north to south.

Fig. 2. Field photograph from the Hällekis quarry, north-western Kinnekulle, Västergötland, south-central Sweden. Rock units referred to in the main text are indicated.

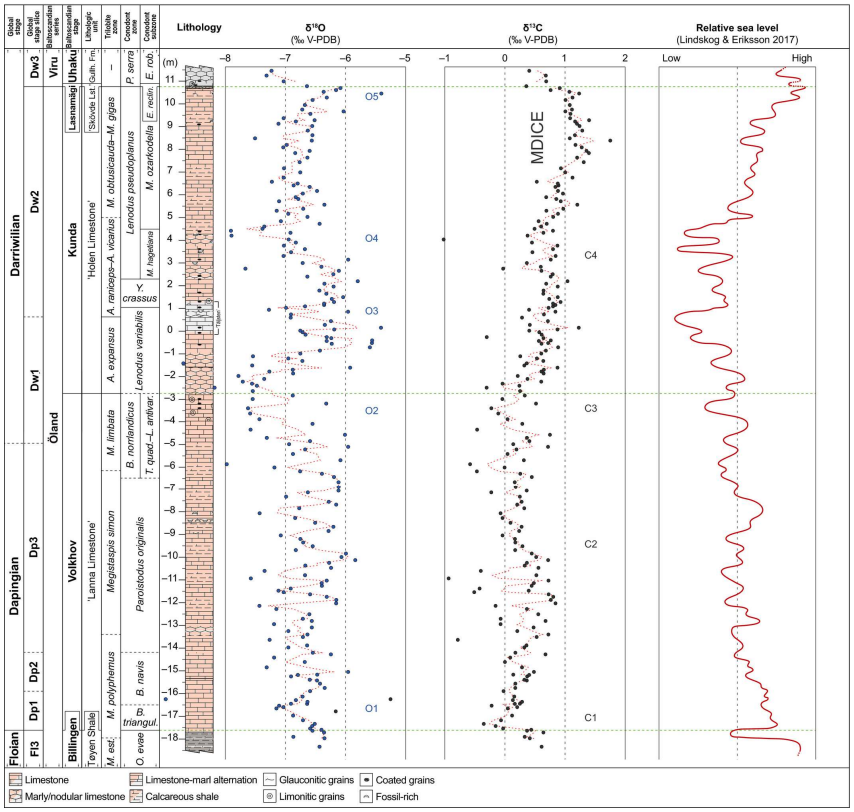

Fig. 3. Sedimentary profile of the 'orthoceratite limestone' and enclosing strata at the Hällekis quarry (modified from Lindskog & Eriksson 2017). Carbon ($\delta^{13}C_{carb}$) and oxygen ($\delta^{18}O_{carb}$) isotope curves are plotted together with an interpretation of relative sea level *sensu* Lindskog & Eriksson (2017). Two-point moving averages (stippled line; calculated from base) are indicated. Biostratigraphy after Tjernvik (1956), Zhang (1998a, b), Bergström & Löfgren (2009), Mellgren & Eriksson (2010), Schmitz et al. (2010) and Lindskog et al. (2014), with the middle part of the 'Lanna Limestone' extrapolated from Nielsen (1995) and Löfgren (1995).

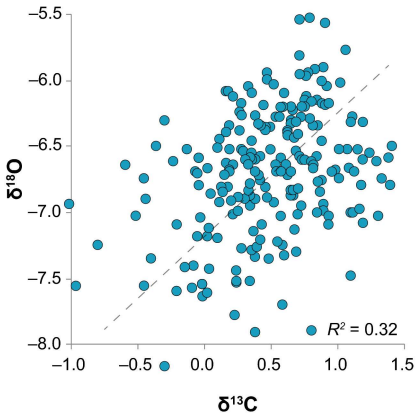

Fig. 4. Cross plot of the $\delta^{13}C$ and $\delta^{18}O$ data with linear (least-squares regression) trend line indicated.

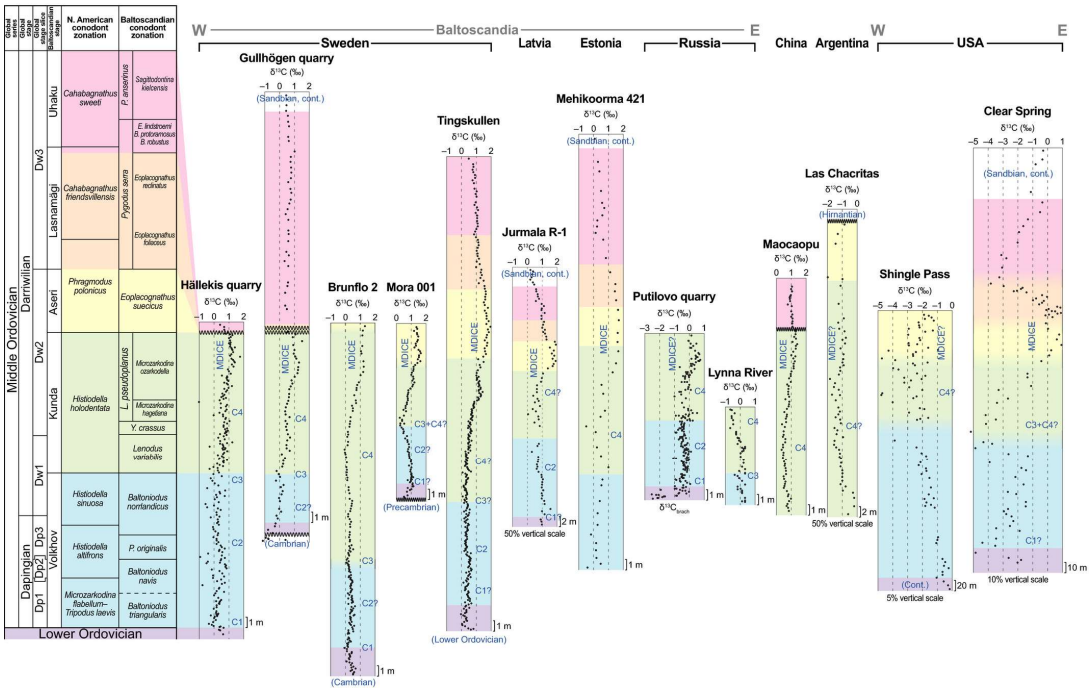

Fig. 5. Comparison between the carbon isotope ($\delta^{13}C_{carb}$) curve at Hällekis with (portions of) select $\delta^{13}C_{carb}$ curves from other localities (Gullhögen quarry, outcrop: Meidla et al. 2004; Brunflo 2, drill core: Wu et al. 2017; Mora 001, drill core; Lehnert et al. 2014; Tingskullen, drill core: Wu et al. 2017; Jurmala R-1, drill core: Ainsaar et al. 2004; Mehikoorma 421, drill core: Kaljo et al. 2007; Putilovo quarry, outcrop: Rasmussen et al. 2016; Lynna River, outcrop: Zaitsev & Pokrovsky 2014; Maocaopu, outcrop: Schmitz et al. 2010; Las Chacritas, outcrop: Albanesi et al. 2013; Shingle Pass, outcrop: Edwards & Saltzman 2014; Clear Spring, outcrop: Saltzman & Edwards 2017). All sections are shown to the same vertical scale (i.e., their relative thicknesses are represented correctly), except where noted. Colour coding indicates biostratigraphic correlation as tied to the Baltoscandian stratigraphic framework (modified from Lindskog et al. 2017); graded transitions indicate uncertain boundaries (biostratigraphic data from Jaanusson & Mutvei 1951; Jaanusson 1964; Karis 1998; Zhang 1998a; Löfgren 2003; Ainsaar et al. 2004; Meidla et al. 2004; Bergström 2007; Kaljo et al. 2007; Schmitz et al. 2010; Albanesi et al. 2013; Edwards & Saltzman 2014; Rasmussen et al. 2016; Lindskog & Eriksson 2017; Saltzman & Edwards 2017; Wu et al. 2017; see further references therein).

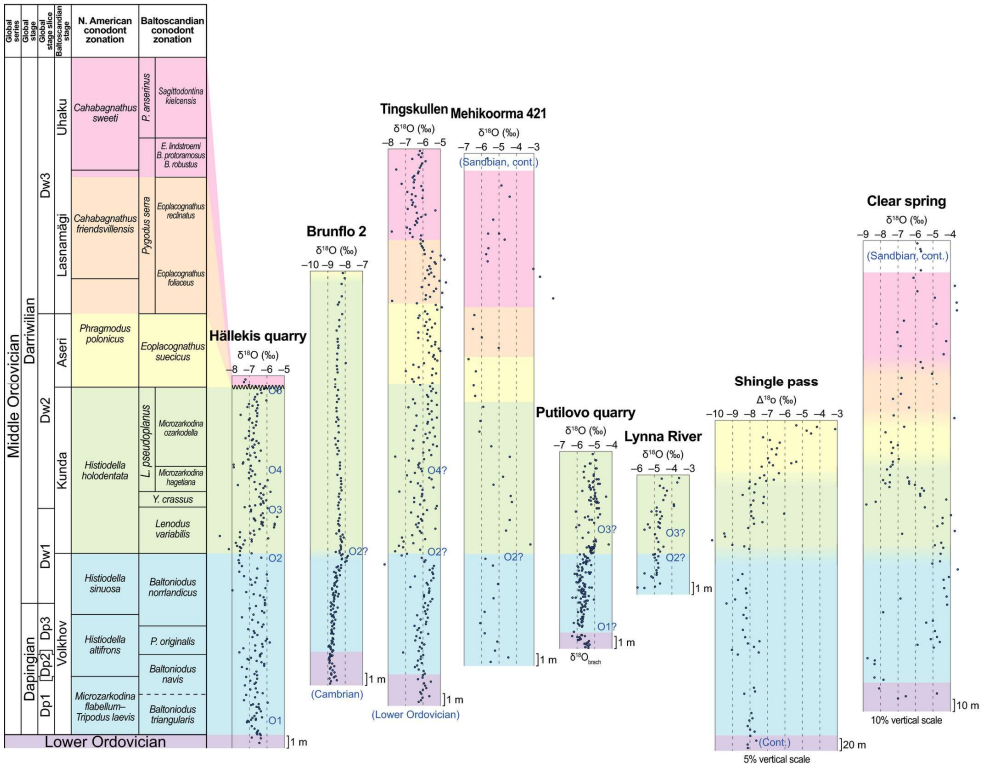

Fig. 6. Comparison between the oxygen ($\delta^{18}O_{carb}$) isotope curve at Hällekis with select $\delta^{18}O_{carb}$ curves from other localities (from works providing both $\delta^{13}C$ and $\delta^{18}O$ data sets). All sections are shown to the same vertical scale, except where noted. Colour coding indicates biostratigraphic correlation as tied to the Baltoscandian stratigraphic framework; graded transitions indicate uncertain boundaries. For references, see Fig. 5.

Table 1. List of samples, in stratigraphic order, and their $\delta^{13}C_{carb}$ and $\delta^{18}O_{carb}$ values, expressed as ‰ relative to the Vienna Pee Dee Belemnite. The stratigraphic position of the respective samples can be found in Lindskog & Eriksson (2017, figures 6, 7).

Gullhögen Formation	HÄ12-ÖP4	0.42	−7.21
Gullhögen Formation	HÄ12-ÖP3	0.69	−7.30
Gullhögen Formation	HÄ12-ÖP2	0.70	−7.02
‘Skövde Limestone’	HÄ12-ÖP1	0.37	−6.60
‘Holen Limestone’	HÄ12-ÖP5	0.92	−6.05
‘Holen Limestone’	HÄ12-ÖP6	0.75	−6.15
‘Holen Limestone’	HÄ12 ÖP7	1.10	−6.32
‘Holen Limestone’	HÄ12 ÖP8	1.25	−5.35
‘Holen Limestone’	HÄ12 ÖP9	1.11	−6.27
‘Holen Limestone’	HÄ15-1	1.01	−6.52
‘Holen Limestone’	HÄ15-2	1.08	−6.66
‘Holen Limestone’	HÄ15-3	1.13	−6.69
‘Holen Limestone’	HÄ12 ÖP10	1.02	−6.01
‘Holen Limestone’	HÄ15-4	1.07	−6.52
‘Holen Limestone’	HÄ15-5	1.10	−7.00
‘Holen Limestone’	HÄ12 ÖP11	1.40	−6.49

‘Holen Limestone’	HÄ15-6	1.18	−6.80
‘Holen Limestone’	HÄ15-7	1.19	−7.08
‘Holen Limestone’	HÄ15-8	1.24	−6.55
‘Holen Limestone’	HÄ15-9	1.29	−6.62
‘Holen Limestone’	HÄ15-10	1.15	−6.52
‘Holen Limestone’	HÄ12-ÖP12	1.10	−7.48
‘Holen Limestone’	HÄ15-11	1.76	−6.53
‘Holen Limestone’	HÄ15-12	1.16	−6.97
‘Holen Limestone’	HÄ15-13	1.30	−7.03
‘Holen Limestone’	HÄ12 ÖP13	1.38	−6.59
‘Holen Limestone’	HÄ15-14	1.39	−6.80
‘Holen Limestone’	HÄ15-15	1.19	−6.60
‘Holen Limestone’	HÄ15-16	1.33	−6.74
‘Holen Limestone’	HÄ15-17	0.93	−7.03
‘Holen Limestone’	HÄ15-18	1.01	−6.74
‘Holen Limestone’	HÄ15-19	1.11	−7.00
‘Holen Limestone’	HÄ12-38	0.54	−7.22
‘Holen Limestone’	HÄ15-20	0.87	−6.76
‘Holen Limestone’	HÄ12-37	0.87	−6.84
‘Holen Limestone’	HÄ15-21	0.84	−6.57
‘Holen Limestone’	HÄ12-36	0.88	−6.45
‘Holen Limestone’	HÄ15-22	0.95	−6.69
‘Holen Limestone’	HÄ15-23	0.71	−6.82
‘Holen Limestone’	HÄ12-35	0.85	−6.77
‘Holen Limestone’	HÄ15-24	0.93	−7.09
‘Holen Limestone’	HÄ15-25	1.19	−6.32
‘Holen Limestone’	HÄ15-26	0.98	−6.67
‘Holen Limestone’	HÄ12-34	0.67	−7.13
‘Holen Limestone’	HÄ15-27	0.90	−6.94
‘Holen Limestone’	HÄ15-28	0.80	−6.61
‘Holen Limestone’	HÄ12-33	0.57	−7.03
‘Holen Limestone’	HÄ15-29	0.68	−6.43
‘Holen Limestone’	HÄ12-32	0.60	−7.33
‘Holen Limestone’	HÄ12-31	0.48	−7.35
‘Holen Limestone’	HÄ12-30	0.80	−7.90
‘Holen Limestone’	HÄ12-29	0.66	−6.87
‘Holen Limestone’	HÄ12-28	0.38	−7.90
‘Holen Limestone’	HÄ12-27	−1.03	−6.93
‘Holen Limestone’	HÄ12-26	0.46	−6.81
‘Holen Limestone’	HÄ12-25	0.89	−6.99
‘Holen Limestone’	HÄ12-24	0.81	−6.64

‘Holen Limestone’	HÄ12-23	0.46	−6.88
‘Holen Limestone’	HÄ12-22	0.84	−7.00
‘Holen Limestone’	HÄ12-21	0.78	−5.94
‘Holen Limestone’	HÄ12-20	0.38	−6.70
‘Holen Limestone’	HÄ15-30	0.63	−6.38
‘Holen Limestone’	HÄ12-19	−0.02	−7.64
‘Holen Limestone’	HÄ15-31	0.60	−6.09
‘Holen Limestone’	HÄ15-32	0.80	−6.16
‘Holen Limestone’	HÄ12-18	0.75	−6.60
‘Holen Limestone’	HÄ12-17	1.05	−5.77
‘Holen Limestone’	HÄ12-16	0.69	−6.31
‘Holen Limestone’	HÄ12-15	0.90	−6.18
‘Holen Limestone’	HÄ12-14	0.63	−6.42
‘Holen Limestone’	HÄ12-13	0.65	−6.31
‘Holen Limestone’	HÄ12-12	0.87	−6.01
‘Holen Limestone’	HÄ15-33	0.72	−6.19
‘Holen Limestone’	HÄ15-34	0.93	−6.17
‘Holen Limestone’	HÄ12-11	0.82	−6.34
‘Holen Limestone’	HÄ15-35	0.85	−6.34
‘Holen Limestone’	HÄ15-36	0.81	−6.66
‘Holen Limestone’	HÄ12-10	0.72	−6.95
‘Holen Limestone’	HÄ12-9	0.39	−7.26
‘Holen Limestone’	HÄ12-8	0.83	−5.91
‘Holen Limestone’	HÄ12-7	0.65	−6.87
‘Holen Limestone’	HÄ12-6	0.30	−6.90
‘Holen Limestone’	HÄ12-5	0.75	−6.20
‘Holen Limestone’	HÄ12-4	0.41	−6.33
‘Holen Limestone’	HÄ12-3	1.24	−5.39
‘Holen Limestone’	HÄ12-2	0.88	−6.18
‘Holen Limestone’	HÄ12-1	0.40	−6.72
‘Holen Limestone’	HÄ12-39	0.57	−6.69
‘Holen Limestone’	HÄ12-40	0.61	−6.63
‘Holen Limestone’	HÄ12-41	−0.30	−6.30
‘Holen Limestone’	HÄ15-37	0.64	−6.19
‘Holen Limestone’	HÄ12-42	0.79	−5.52
‘Holen Limestone’	HÄ15-38	0.56	−6.27
‘Holen Limestone’	HÄ12-43	0.72	−5.54
‘Holen Limestone’	HÄ15-39	0.59	−6.20
‘Holen Limestone’	HÄ15-40	0.90	−5.57
‘Holen Limestone’	HÄ12-44	0.70	−6.41
‘Holen Limestone’	HÄ12-45	0.62	−6.72

‘Holen Limestone’	HÄ12-46	0.24	−7.52
‘Holen Limestone’	HÄ12-47	0.52	−6.92
‘Holen Limestone’	HÄ12-48	0.65	−6.69
‘Holen Limestone’	HÄ12-49	0.35	−8.68
‘Holen Limestone’	HÄ12-50	0.34	−7.52
‘Holen Limestone’	HÄ12-51	0.90	−5.90
‘Holen Limestone’	HÄ12-52	0.65	−6.84
‘Holen Limestone’	HÄ12-53	0.59	−7.24
‘Holen Limestone’	HÄ12-54	0.66	−6.84
‘Holen Limestone’	HÄ12-55	0.23	−7.77
‘Holen Limestone’	HÄ12-56	0.38	−7.34
‘Holen Limestone’	HÄ12-57	0.59	−7.69
‘Holen Limestone’	HÄ12-58	−0.02	−7.55
‘Holen Limestone’	HÄ12-59	0.23	−7.43
‘Holen Limestone’	HÄ12-60	−0.30	−8.16
‘Holen Limestone’	HÄ12-61	0.23	−7.52
‘Lanna Limestone’	HÄ12-62	0.34	−6.87
‘Lanna Limestone’	HÄ12-63	−0.02	−7.54
‘Lanna Limestone’	HÄ12-64	0.53	−6.27
‘Lanna Limestone’	HÄ12-65	−0.21	−7.60
‘Lanna Limestone’	HÄ12-66	−0.10	−7.57
‘Lanna Limestone’	HÄ12-67	0.03	−7.42
‘Lanna Limestone’	HÄ12-68	0.27	−6.52
‘Lanna Limestone’	HÄ12-69	−0.46	−7.56
‘Lanna Limestone’	HÄ12-70	0.76	−5.96
‘Lanna Limestone’	HÄ12-71	0.36	−7.28
‘Lanna Limestone’	HÄ12-72	0.42	−6.58
‘Lanna Limestone’	HÄ12-73	0.11	−6.92
‘Lanna Limestone’	HÄ12-74	0.71	−5.95
‘Lanna Limestone’	HÄ12-75	0.22	−6.64
‘Lanna Limestone’	HÄ12-76	0.04	−6.86
‘Lanna Limestone’	HÄ12-77	0.33	−6.05
‘Lanna Limestone’	HÄ12-78	−0.59	−6.63
‘Lanna Limestone’	HÄ12-79	0.02	−7.18
‘Lanna Limestone’	HÄ12-80	−0.45	−6.75
‘Lanna Limestone’	HÄ12-81	0.26	−6.38
‘Lanna Limestone’	HÄ12-82	0.44	−6.19
‘Lanna Limestone’	HÄ12-83	0.18	−6.08
‘Lanna Limestone’	HÄ12-84	0.17	−6.08
‘Lanna Limestone’	HÄ12-85	0.35	−6.09
‘Lanna Limestone’	HÄ12-86	−0.23	−6.62

‘Lanna Limestone’	HÄ12-87	0.25	−6.98
‘Lanna Limestone’	HÄ12-88	0.28	−6.26
‘Lanna Limestone’	HÄ12-89	0.22	−6.12
‘Lanna Limestone’	HÄ12-90	0.34	−6.78
‘Lanna Limestone’	HÄ12-91	−0.08	−7.40
‘Lanna Limestone’	HÄ12-92	−0.05	−6.79
‘Lanna Limestone’	HÄ12-93	0.10	−6.51
‘Lanna Limestone’	HÄ12-94	0.27	−6.18
‘Lanna Limestone’	HÄ12-95	0.27	−6.24
‘Lanna Limestone’	HÄ12-96	−0.03	−7.04
‘Lanna Limestone’	HÄ12-97	0.15	−6.72
‘Lanna Limestone’	HÄ12-98	0.19	−6.67
‘Lanna Limestone’	HÄ12-99	0.29	−6.53
‘Lanna Limestone’	HÄ12-100	0.18	−6.80
‘Lanna Limestone’	HÄ12-101	0.46	−5.99
‘Lanna Limestone’	HÄ12-102	0.52	−6.03
‘Lanna Limestone’	HÄ12-103	0.71	−5.81
‘Lanna Limestone’	HÄ12-104	0.37	−6.26
‘Lanna Limestone’	HÄ12-105	0.32	−6.64
‘Lanna Limestone’	HÄ12-106	0.58	−6.20
‘Lanna Limestone’	HÄ12-107	−0.40	−7.34
‘Lanna Limestone’	HÄ12-108	0.53	−6.64
‘Lanna Limestone’	HÄ12-109	−0.97	−7.55
‘Lanna Limestone’	HÄ12-110	0.73	−6.28
‘Lanna Limestone’	HÄ12-111	0.49	−6.36
‘Lanna Limestone’	HÄ12-112	0.46	−6.36
‘Lanna Limestone’	HÄ12-113	−0.44	−6.90
‘Lanna Limestone’	HÄ12-114	0.43	−7.09
‘Lanna Limestone’	HÄ12-115	−0.52	−7.02
‘Lanna Limestone’	HÄ12-116	0.71	−6.57
‘Lanna Limestone’	HÄ12-117	0.79	−6.29
‘Lanna Limestone’	HÄ12-118	0.76	−6.13
‘Lanna Limestone’	HÄ12-119	0.85	−6.15
‘Lanna Limestone’	HÄ12-120	−0.14	−7.42
‘Lanna Limestone’	HÄ12-121	0.36	−7.14
‘Lanna Limestone’	HÄ12-122	0.57	−6.59
‘Lanna Limestone’	HÄ12-123	−0.07	−6.69
‘Lanna Limestone’	HÄ12-124	0.68	−6.54
‘Lanna Limestone’	HÄ12-125	−0.05	−7.19
‘Lanna Limestone’	HÄ15-41	0.50	−6.53
‘Lanna Limestone’	HÄ12-126	0.20	−6.92

‘Lanna Limestone’	HÄ15-42	0.72	−6.60
‘Lanna Limestone’	HÄ12-127	0.53	−6.69
‘Lanna Limestone’	HÄ12-128	−0.80	−7.24
‘Lanna Limestone’	HÄ15-43	0.35	−6.59
‘Lanna Limestone’	HÄ12-129	0.34	−6.94
‘Lanna Limestone’	HÄ15-44	0.18	−6.52
‘Lanna Limestone’	HÄ12-130	0.67	−6.22
‘Lanna Limestone’	HÄ12-131	0.10	−7.19
‘Lanna Limestone’	HÄ12-132	0.02	−6.66
‘Lanna Limestone’	HÄ12-133	0.27	−7.27
‘Lanna Limestone’	HÄ12-134	0.47	−5.94
‘Lanna Limestone’	HÄ12-135	0.11	−6.45
‘Lanna Limestone’	HÄ15-C6	0.42	−6.76
‘Lanna Limestone’	HÄ15-C5	0.38	−6.89
‘Lanna Limestone’	HÄ15-C1	0.34	−6.58
‘Lanna Limestone’	HÄ15-45	0.35	−6.46
‘Lanna Limestone’	HÄ15-B1	0.17	−6.40
‘Lanna Limestone’	HÄ15-B2	0.19	−6.34
‘Lanna Limestone’	HÄ15-B3	−0.04	−6.58
‘Lanna Limestone’	HÄ15-B4	0.19	−6.70
‘Lanna Limestone’	HÄ15-C2	−1.89	−9.02
‘Lanna Limestone’	HÄ15-D12	0.13	−6.80
‘Lanna Limestone’	HÄ15-B5	0.31	−6.60
‘Lanna Limestone’	HÄ15-C3	0.25	−6.88
‘Lanna Limestone’	HÄ15-D11	0.16	−6.63
‘Lanna Limestone’	HÄ15-D10	−0.21	−7.10
‘Lanna Limestone’	HÄ15-C4	0.22	−7.02
‘Lanna Limestone’	HÄ15-D9	0.04	−7.12
‘Lanna Limestone’	HÄ15-D8	−2.83	−17.07
‘Lanna Limestone’	HÄ15-D7	0.13	−6.85
‘Lanna Limestone’	HÄ15-D6	−0.06	−6.70
‘Lanna Limestone’	HÄ15-D5	−0.37	−6.49
‘Lanna Limestone’	HÄ15-D4	−0.13	−6.52
‘Lanna Limestone’	HÄ15-D3	−0.05	−6.58
‘Lanna Limestone’	HÄ15-D2	0.45	−6.38
‘Lanna Limestone’	HÄ15-D1	0.36	−6.55
Tøyen Shale	HÄ15-D13	0.65	−6.33
Tøyen Shale	HÄ15-D14	0.33	−6.83
Tøyen Shale	HÄ15-D15	0.41	−6.34
Tøyen Shale	HÄ15-D16	0.62	−6.40